Supporting Information

A hybrid shell material with mixed ion/electron conductivity used for high-performance Li-S batteries

Huanhuan Li,[a] Zhaofei Ge,[a] Yanping Zheng,[b] Yan Xue,[a] Guangyue Bai,*[a] Jianji Wang,[a] Kelei Zhuo,[a] and Yujie Wang*[c]

[a]*Collaborative Innovation Center of Henan Province for Green Manufacturing of Fine Chemicals, Key Laboratory of Green Chemical Media and Reactions, Ministry of Education, School of Chemistry and Chemical Engineering, Henan Normal University, Xinxiang, Henan 453007, PR China.*

E-mail: baiguangyue@htu.cn.

[b]*Faculty of Chemistry, Tonghua Normal University, Tonghua, Jilin 134002, China.*

[c]*School of Chemistry and Chemical Engineering, Henan Institute of Science and Technology, Xinxiang, P. R. China. E-mail:yujiewang2001@163.com.*

Experimental Procedures

Synthesis of Hollow Nb₂O₅ microspheres (m-Nb₂O₅). All the chemicals were directly used after purchase without further purification. The initial hollow m-Nb_2O_5 was synthesized via a modified hydrothermal method followed with heat-treatment.[1] Typically, 0.684 g of formaldehyde and 0.924 g of ammonium niobate oxalate hydrate were mixed and dissolved in 35 mL of DI-water at room temperature. The well mixed solution was then heated at 40 °C for 5 h in an oil bath. Finally, the solution was transferred to a Teflon-lined autoclave and heated at 175 °C for 24 h to obtain Nb_2O_5@ploymer core-shell microspheres. Finally, after calcination in air atmosphere for 2 h at 600 °C, the white m-Nb_2O_5 was obtained.

Synthesis of hybrid shell of m-Nb₂O₅@rGO. To prepare composite of m-Nb_2O_5@rGO, the surface of m-Nb_2O_5 was first modified by positive charged PDDA. And then, the GO aqueous solution with negative Zeta potential was added drop by drop. The mass of S@m-Nb_2O_5 and GO used in self-assembling were 100 and 15 mg, respectively. After ultrasonication for 8 min, light yellow m-Nb_2O_5@GO was obtained. At last, the m-Nb_2O_5@GO was sealed in a tube furnace, and heated at 700 °C for 3 h under a Ar/H_2 atmosphere. And after the thermal reduction of GO, the gray m-Nb_2O_5@rGO was finally obtained.

Preparation of S@m-Nb₂O₅ and S@m-Nb₂O₅@rGO. First, mixed the m-Nb_2O_5@rGO and sulfur power with the weight ratio of 1:6. Herein, the mass of m-Nb_2O_5@rGO using in sulfur infiltration was 80 mg. Then sealed the mixture in a glass vessel under argon protection, and heated at 300 °C for 5 h in a tube furnace for introduceing sulfur into hollow m-Nb_2O_5@rGO. After cooling down to room temperature, S@m-Nb_2O_5@rGO was obtained. For a fair comparison, the preparation process of S@m-Nb_2O_5 is the same with the above mentioned method to keep sulfur contents in both S@m-Nb_2O_5@rGO and S@m-Nb_2O_5 are around 72 wt%.

Materials characterization

The morphologies and structures of produced materials were characterized by field-emission scanning electron microscopy (FESEM; JSM-6390LV) and transmission electron microscopy (TEM; JEOL, JEM 2100). Crystal structures and phase purity of samples were determined by Powder X-ray diffraction (XRD) conducted on Bruker-D8 ADVANCE (Germany) with a Cu Kα radiation (λ=1.5418 Å). Elemental mapping was collected using EDX spectroscopy attached to FESEM. Thermogravimetric analysis (TGA) measurements were performed using a STA449C instrument. X-ray photoelectron spectroscopy (XPS) was carried out on ESCALAB250Xi with an Al Kα source. The UV−vis absorption spectrum of the solution was acquired by an ultraviolet and visible spectrophotometer (Lambd 950). Zeta potential was conducted on the ZETASIZER (Malvern, Nano-ZS90).

Electrochemical measurements

To make the cathode electrode for Li-S batteries, the active material powder (80 wt%), CB (10 wt%), and PVDF binder (10 wt%) were mixed in N-methyl pyrrolidone (NMP) to form a slurry. And then the slurry was coated on the aluminum foil and dried at 60 °C overnight. The mass loading of the electrode material is ~3.04 mg cm^{-2}.The CR 2032 coin cells were assembled in an argon-filled glove box using lithium foil as the counter

electrode and 1.0 M lithium bis(trifluoromethanesulfonyl) imide in a mixture of 1,3-dioxolane and dimethoxymethane (1:1, v/v) containing 0.5 M of $LiNO_3$ as the electrolyte. Galvanostatic discharge-charge tests were performed on a LAND CT2001A battery-testing instrument within the voltage of 1.7-2.8 V. Specific capacity was calculated based on the mass of sulfur in the composite determined by TGA (1C = 1675 mA g^{-1}). Cyclic voltammetry (CV) of the electrode was conducted on the CHI660E electrochemical station. EIS tests with coin cells were carried out at in the frequency of 100 kHz to 10 mHz at the open-circuit voltage with aperturbation amplitude of 5 mV. To carry out the visualized UV-vis adsorption test, Li_2S_4 solution was prepared according to the literature.[2] In a typical process, S powder and solid Li_2S was mixed at a molar ratio of 1:3 and then dissolved in dimethoxymethane followed by vigorous magnetic stirring at 60 °C. After stirring for 24 h, the light brown Li_2S_4 solution was obtained.

Computational method

Based on density functional theory(DFT), the theoretical calculations were carried out using the Vienna ab initio Simulation Package (VASP). Projector augmented wave (PAW) method and Generalized-gradient approximation (GGA) with the functional of Perdew-Burke-Ernzerhof (PBE) were used in DFT calculations. The binding energy (E_b) between LPSs, Li_2S species and Nb_2O_5 (001) surface was defined as following:

$$E_b=E_{\alpha\beta}-E_\alpha-E_\beta$$

where $E_{\alpha\beta}$ is total energies of the adsorbed system. E_α and E_β are the energies of substrate system and LPSs or Li_2S, respectively.
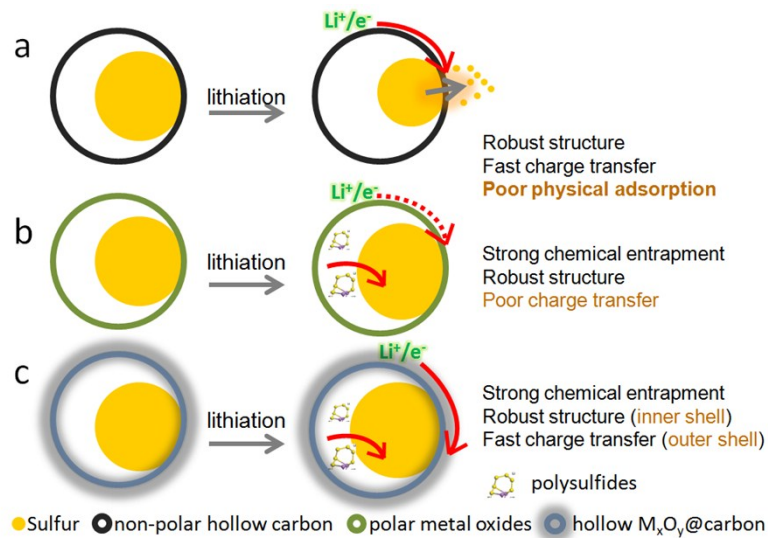
Figure S1. Schematic of the advantages and disadvantages in various yolk-shell structured sulphur-based materials. (a) The common non-polar shell undergoes poor adsorption to lithium-polysulfides (LPSs), resulting in capacity decay and low coulombic efficiency. (b) Although the polar metal oxide shell provides a strong chemical entrapment to LPSs, poor electroconductivity metal oxides leads to poor rate performance. (c) The hybrid shell materials that containing both a highly conductive layer and fast Li-motion property, as well as moderate chemical adsorption to LPSs, can well solve the main issues related to LSBs origining from its underlying conversion chemistry, such as the poor electronic/ionic conductivity of sulfur, the shuttle effect of LPSs, and the volumetric variation of sulfur during cycling processes.
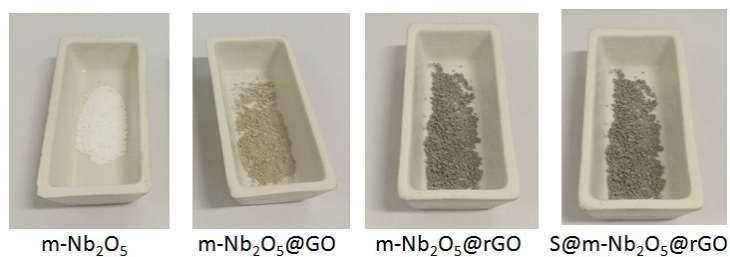

Figure S2. Optical photos of the obtained hollow m-Nb_2O_5, m-Nb_2O_5@GO, m-Nb_2O_5@rGO, and S@m-Nb_2O_5@rGO, respectively.
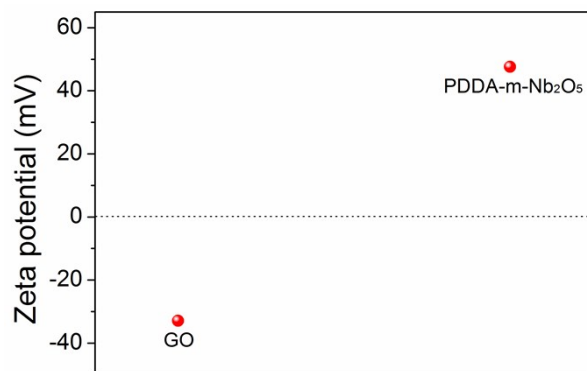
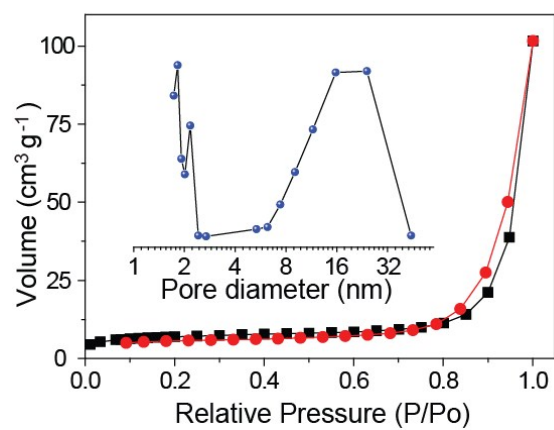**Figure S3.** Zeta-potential results of suspensions of GO and PDDA-m-Nb$_2$O$_5$.

Figure S4. Nitrogen adsorption−desorption isotherms and its pore size distribution curve of the prepared hollow m-Nb$_2$O$_5$ microsspheres. The isotherms of the m-Nb$_2$O$_5$ microsspheres yield a relatively high specific surface area of 97.8 m^2 g^{-1} and a wide pore size distribution centering around 2-30 nm.
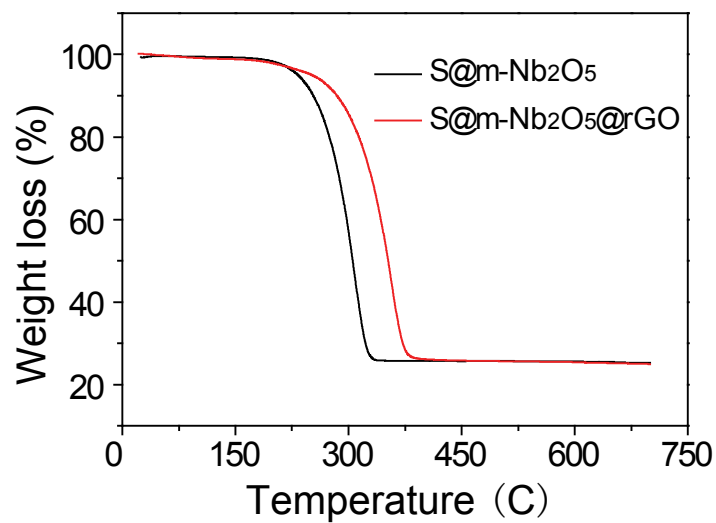
Figure S5. TGA curves under nitrogen atmosphere for S@m-Nb$_2$O$_5$@rGO and S@m-Nb$_2$O$_5$, respectively.
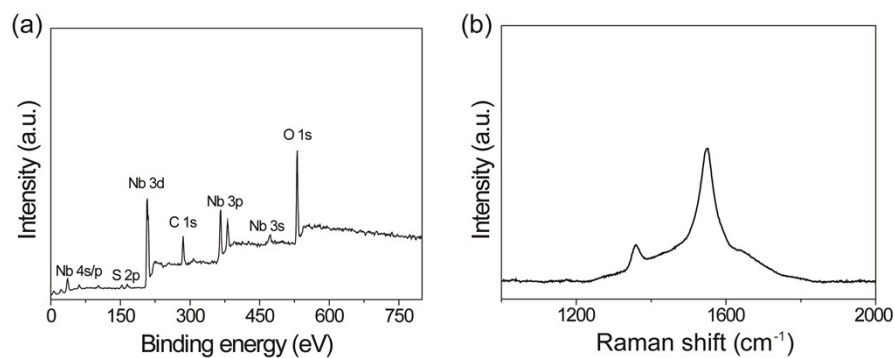

Figure S6. (a) The broad spectrum of S@m-Nb$_2$O$_5$@rGO reveals the existence of niobium, oxygen, carbon and sulfur elements. (b) As a typical class of rGO sehll in the S@m-Nb$_2$O$_5$@rGO composite is verified by Raman spectroscopy with two bands around 1580 cm^{-1} (graphitic carbon) and 1360 cm^{-1} (disordered carbon).
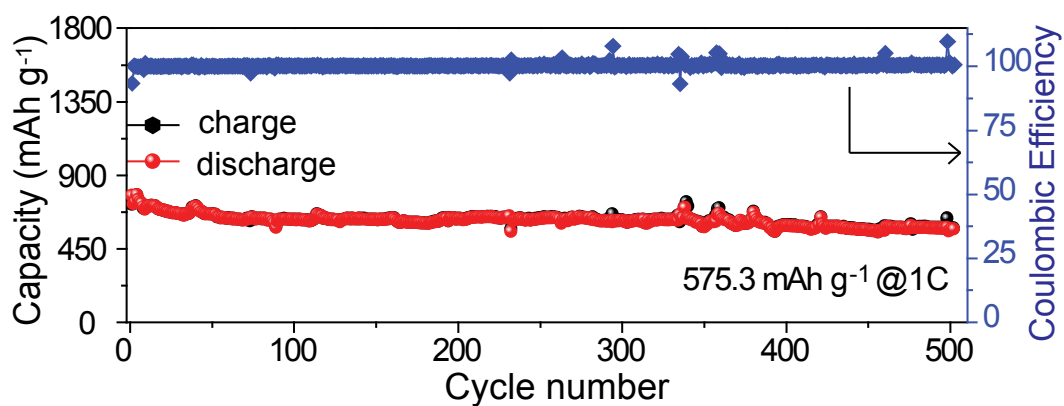
Figure S7. Long cycle performance of S@m-Nb$_2$O$_5$@rGO at a high current density of 1C. Reversible capacity at 1 C of S@m-Nb$_2$O$_5$@rGO was 776.7 mA h g-1, and the corresponding capacity decay was 0.041% per cycle during 500 cycles.
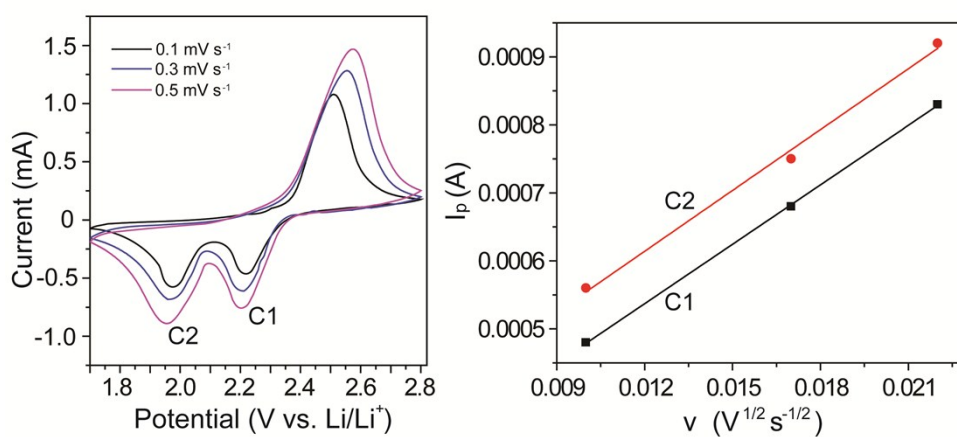

Figure S8. The CV curves at different scan rates and the linear fits of the peak current for the Li-S batteries with the prepared S@m-Nb$_2$O$_5$@rGO as the cathode.
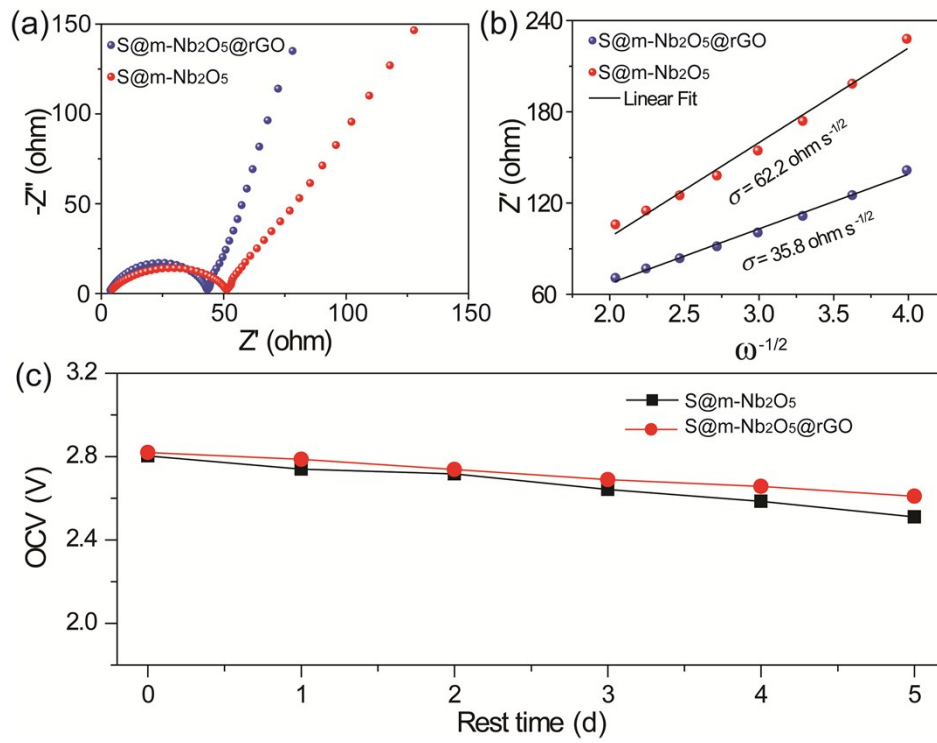
Figure S9. Nyquist plots of lithium sulfur batteries with S@m-Nb$_2$O$_5$ and S@m-Nb$_2$O$_5$@rGO as sulfur hosts at the OCV state.
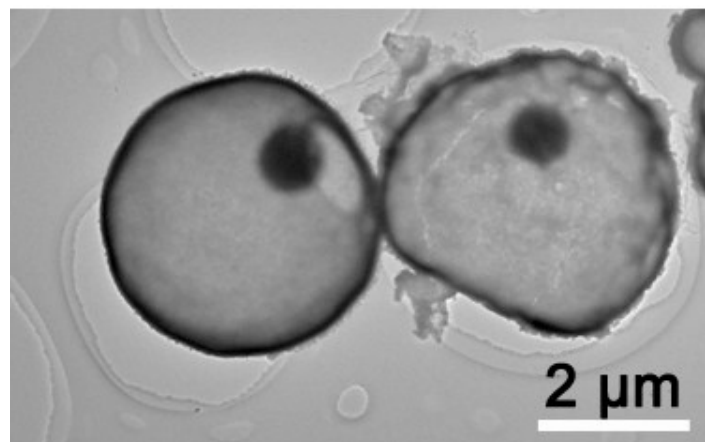

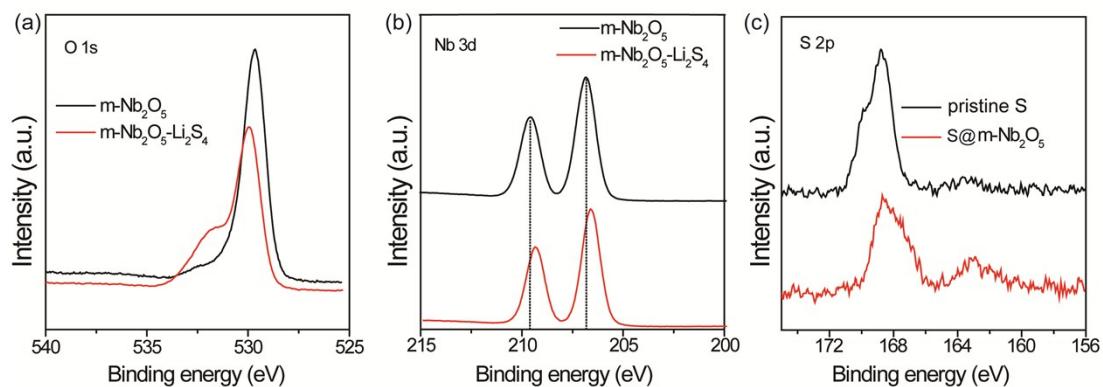**Figure S10.** TEM image of S@m-Nb$_2$O$_5$@rGO after 100 deep cycles at 0.2 C.

Figure S11. XPS spectra of (a) O 1s and (b) Nb 3d of m-Nb_2O_5 before and after absorbing Li_2S_4, as well as the spectra of S 2p for pristine sulfur and S@m-Nb_2O_5 composite. Significant differences can be found in the O and Nb peaks after absorbing Li_2S_4, suggesting m-Nb_2O_5 absorbing Li_2S_4 make electron cloud density around O and Nb atoms in m-Nb_2O_5 change, thus strongly proving that there was chemisorption between LPSs and m-Nb_2O_5. In addition, no obvious difference between the S2p XPS spectra of pristine sulfur and S@m-Nb_2O_5 composite can be found, suggesting no formation of covalent S–Nb bonds.

Table S1. Comparison of cycling and rate performances of the prepared m-Nb_2O_5@rGO with other high performance matrices used in lithium sulfur batteries.

Matrix	Cycle performance	Rate performance	Ref.
	724.5 mAh g^{-1}@0.2C after 200 cycles	931/853/801/633 mAh g^{-1} @0.2C/0.5C/1C/2C	3
TiO_2/$BaTiO_3$ heterostructure	541/493 mAh g^{-1}@0.5C/5C after 500/500 cycles,	842/704/607/493 mAh g^{-1} @0.5C/1C/2C/5C	4
C@TiO_2@C hollow microspheres	740/511 mAh g^{-1}@0.5C/2C after 300/500 cycles,	774 mAh g^{-1}@ 2C	5
TiO_2 nanowires	548 mAh g^{-1}@1C after 300 cycles	1325/918/710/510 mAh g^{-1} @0.1C/0.5C/1C/2C	6
MoS2@hierarchical carbon spheres	643 mAh g^{-1}@0.5C after 500 cycles	1047/902/775/700 mAh g^{-1} @0.2C/0.5C/1C/2C	7
MoN-VN Heterostructure	555 mAh g^{-1}@1C after 500 cycles	1156/988/870/636 mAh g^{-1} @0.2C/0.5C/1C/2C	8
hollow MoO_2 sphere/nitrogen-doped graphene	664 mAh g^{-1}@1C after 500 cycles	1049/876/746/615 mAh g^{-1} @0.2C/0.5C/1C/2C	9
m-Nb_2O_5@rGO	923.1/575.3 mAh g^{-1}@0.2C/1C after 200/500 cycles	1004.5/812.5/562.1/429.1 mAh g^{-1} @ 0.2C/0.5C/2C/3C	This work

References

1. L. Kong, C. Zhang, J. Wang, W. Qiao, L. Ling and D. Long, *Sci. Rep.,* 2016, **6**, 21177.

2. L. Zhang, X. Chen, F. Wan, Z. Niu, Y. Wang, Q. Zhang and J. Chen, *ACS Nano*, 2018, **12**, 9578.

3. J. Zhang, Z. Li, Y. Chen, S. Gao and X. W. D. Lou, *Angew. Chem. Int. Ed. Engl.*, 2018, **57**, 10944.

4. H.-E. Wang, K. Yin, X. Zhao, N. Qin, Y. Li, Z. Deng, L. Zheng, B.-L. Su and Z. Lu, *Chem. Commun.*, 2018, **54**, 12250.

5. M. Fang, Z. Chen, Y. Liu, J. Quan, C. Yang, L. Zhu, Q. Xu and Q. Xu, *J. Mater. Chem. A*, 2018, **6**, 1630.

6. Y. Yan, T. Lei, Y. Jiao, C. Wu and J. Xiong, *Electrochim. Acta*, 2018, **264**, 20.

7. L. Hu, C. Dai, J.-M. Lim, Y. Chen, X. Lian, M. Wang, Y. Li, P. Xiao, G. Henkelman and M. Xu, *Chem. Sci.*, 2018, **9**, 666.

8. C. Ye, Y. Jiao, H.-Y. Jin, A. Slattery, K. Davey, H.-H. wang and S. Qiao, *Angew. Chem. Int. Ed.*, 2018, **57**, 16703.

9. X. Wu, Y. Du, P. Wang, L. Fan, J. Cheng, M. Wang, Y. Qiu, B. Guan, H. Wu, N. Zhang and K. Sun, *J. Mater. Chem. A*, 2017, **5**, 25187.